Eur. Phys. J. D **22**, 521–526 (2003)
DOI: 10.1140/epjd/e2003-00002-4

THE EUROPEAN PHYSICAL JOURNAL D

Retrieval of spatial shot-noise in the full dynamic range of calibrated CCD cameras

Y. Jiang[1,2], O. Jedrkiewicz[1], S. Minardi[1], P. Di Trapani[1], A. Mosset[3], E. Lantz[3], and F. Devaux[3,a]

[1] INFM and Department of Chemical, Physical and Mathematical Sciences, University of Insubria, Via Valleggio 11, 22100 Como, Italy
[2] Department of Electronic Science and Applied Physics, Fuzhou university 350002, P.R. China
[3] Laboratoire d'Optique P.M. Duffieux[b], Université de Franche-Comté, UFR des Sciences et Techniques, route de Gray, 25030 Besançon Cedex, France

Received 9 September 2002 / Received in final form 16 October 2002
Published online 21 January 2003 –

Abstract. The pixel by pixel calibration of a scientific CCD camera allows Poissonian statistics of the spatial fluctuations of an uniform enlightening to be retrieved in the full range of the camera dynamic. The procedure works efficiently for thermal as well as for laser sources, provided that the wavelength and the coherence properties of the source are chosen in order to avoid the formation of equal thickness fringes in the chip (etaloning effect). Calibration allows also the comparison at the shot noise level of images recorded at different places on the chip.

PACS. 41.85.Ew Beam profile, beam intensity – 42.50.Ar Photon statistics and coherence theory – 42.50.Lc Quantum fluctuations, quantum noise, and quantum jumps – 42.79.-e Optical elements, devices, and systems

1 Introduction

Reducing quantum fluctuations of light in imaging system has recently attracted a considerable interest. Phenomena now well-known in the time-domain have been considered for their counterpart in the spatial domain, leading to effects like noiseless image amplification [1–3], image entanglement [4,5], or generation of multimode squeezing [6,7]. Quantum fluctuations are described by ensemble averages often estimated by time averages, if the signal is stationary in time. However they can also be estimated by spatial averages, if the signal is stationary in space on a sufficiently large area. To study the spatial properties of parametric down-conversion or amplification in the travelling-wave regime for the achievement of two quantum entangled copies of an input image [4,8,9], spatial fluctuations of quantum origin must be correctly retrieved and separated from the classical spatial noise introduced either by the optical system or by the camera. Since the standard shot noise obeys a Poissonian statistics (variance equal to the mean), this quantum noise becomes very low in relative value for high illumination levels and the classical noise, that is in general proportional to the illumination level, could become predominant. Hence, the elimination of spatial classical noise in the maximum range of intensities appears as a prerequisite to demonstrate specific quantum effects below the shot noise level. For example Gatti *et al.* [4] have shown that fluctuations in the intensity difference between an amplified image and its so-called "clone" can be made much below the shot noise. Because both images must be detected simultaneously, any classical noise, resulting in a non equal balance between pixels at the same place in both images, will overcome the detection of sub-shot noise correlations. We show in this paper that the calibration of a scientific CCD camera allows the retrieval of shot-noise statistics in the full dynamic range for a pixel compared with its neighbors as well as for the difference between two images of the same laser beam recorded at different places of the chip.

We present in Section 2 the set-up used for experimental noise measurements. They are performed with two different high-quantum-efficiency CCD cameras and with lamps and lasers as light sources.

We show in Section 3 that the differences between two images recorded in the same conditions exhibit a quasi-perfect Poissonian [10] statistics for intensities in the full dynamic range, as already quoted in [14]. Hence time-domain classical noise can be safely neglected in future experiments where sub-shot noise fluctuations have to be evidenced with CCD cameras, because of their long integration time.

Section 3 involved comparisons between intensities of successive images on each pixel, but not between pixels.

[a] e-mail: fabrice.devaux@univ-fcomte.fr
[b] UMR 6603 CNRS

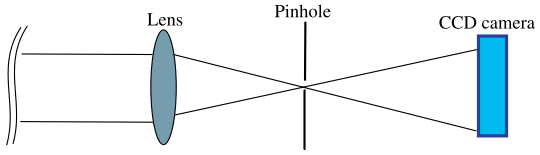

Fig. 1. Experimental setup for calibration of the two CCD cameras.

On the other hand, we show in Section 4 by a comparison between pixels on a small area that spatial classical noise leads to a departure from Poissonian statistics for high levels of a flat-field illumination. This spatial noise originates from pixel to pixel inhomogeneities either in the illumination or in the detection. We show that this noise can be removed by a self-consistent pixel gain calibration method, that allows the retrieval of the Poissonian distribution over the entire dynamic range of both CCD cameras. However, we show that the method fails when fringes of equal thickness are formed in the chip for coherent illumination at wavelengths where silicon is semitransparent (etaloning effect).

To further demonstrate that spatial inhomogeneities were due to the sensitivity of the camera pixels and not to inhomogeneities in the illumination, we show in Section 5 that two images of the same laser beam recorded at two different places of the chip are identical at the Poissonian level after calibration, while they exhibited an excess noise before calibration. Because the illumination used for the calibration (a mercury lamp) was completely different of that used in this section, this is the proof that the pixel-to-pixel inhomogeneity on the CCD chip fully accounts for the measured excess noise.

2 Experimental set-up

Figure 1 shows the experimental set-up used for noise measurement with the CCD cameras. A light beam is focused on a 10 μm pinhole which selects only the central part of the beam thus removing the high-frequency classical noise. Several different light sources were used during the experiments. The CCD camera is put at about 1 m from the pinhole so that the diffraction pattern of the light beam is large compared to the CCD camera chip dimensions (26.8 mm $\times$ 8 mm). Since in the center of the beam the intensity variation is small, the field can be considered flat over a small area of the detection chip (typically of the order of 0.2 mm $\times$ 0.2 mm). Both cameras are based on a back-illuminated, high-quantum efficiency CCD-chips produced by Roper Scientific and have 16 bits dynamical range. The first camera, NTE/CCD-400EHRB-G1 (DDB-CCD, in the following), is a deep depletion back-illuminated CCD characterized by a 95% quantum efficiency (QE) peak centered at the wavelength of 700 nm. The second one, Spec-10:400B (B-CCD, in the following), is a back-illuminated CCD with 90% QE at the wavelength of 527 nm. Both detection arrays have 1 340 $\times$ 400 pixels, and a pixel size of 20 μm $\times$ 20 μm. The deep-depletion CCD is supposed to have less etaloning effect in the near IR spectral region [11]. For experimental testing, cameras are cooled down to -45 °C and -40 °C respectively. As mentioned, the shot-noise measurements were performed with different kinds of light sources. For DDB-CCD camera we use a pulsed ps-laser, white light lamp, and He–Ne laser. The laser pulses are produced in an optical parametric amplifier tuned at 700 nm and pumped by a 1 ps frequency-doubled Nd:Glass laser at 2 Hz repetition rate. For the white light source we use a pocket battery-lamp. In this case, the pin-hole is removed and the light is shone on the camera directly. For B-CCD camera, pulsed lasers and a mercury (Hg) lamp are used as light sources. Laser sources are the second harmonics respectively delivered by a Nd:Glass laser (TWINKLE from Light Conversion Inc.: 527.5 nm wavelength, 1 ps pulse duration, 33 Hz repetition rate) and a Nd:YAG laser (from QUANTEL, 532 nm wavelength, 38 ps pulse duration, 10 Hz repetition rate). With the Hg lamp, a narrow band interferential filter is placed before the pinhole in order to select a single spectral line close to the laser wavelengths. The experiments were respectively carried out in Como and in Besançon.

3 Photon shot-noise measurements: from grey levels to photo-electrons

According to quantum theory, the fluctuations of photon counting over a selected area of a coherent flat-field light beam follow the Poisson distribution. The standard deviation σ for Poisson distribution turns out to be at the shot noise level $\sigma = \sqrt{\overline{n}}$, where $\overline{n}$ is the average photoelectron counting on the selected area. On the other hand, the fluctuations of a thermal light source follow the Bose-Einstein distribution. The standard deviation is given by [12]:

$$\sigma = \sqrt{\overline{n}\left(1 + \frac{\overline{n}}{\mu}\right)}, \tag{1}$$

where $\overline{n}$ is the mean value of the photoelectrons detected on the selected area, $\mu = T/T_c$, where T is the detection time and T_c is the coherence time of the light source. In our experiments, the detection time T is larger than 10 ms and $\overline{n} < 6.5 \times 10^4$ pe. For thermal light, we can assume $T_c \approx 10^{-12}$ s when narrow band interferential filters are used (or $T_c \ll 10^{-12}$ s without filter), so $\overline{n}/\mu \leq 6.5 \times 10^{-5}$. Since $\overline{n}/\mu$ is so small, equation (1) becomes $\sigma \approx \sqrt{\overline{n}}$, *i.e.* it can be approximated by a Poissonian statistic. So the Poissonian statistics should always be satisfied in our experiments, provided that the intensity unit has been converted from gray-levels to photo-electrons (it is well-known that quantum efficiency, that relates the statistics of photons to the statistics of photo-electrons, preserves a Poissonian statistics).

The B-CCD camera was operated in the high gain mode, where the correspondence between gray levels and photoelectrons given by Roper was 0.90 photoelectron/gray level. We checked this value by using the method described in [14]: we recorded in the same conditions two successive images of an uniform background

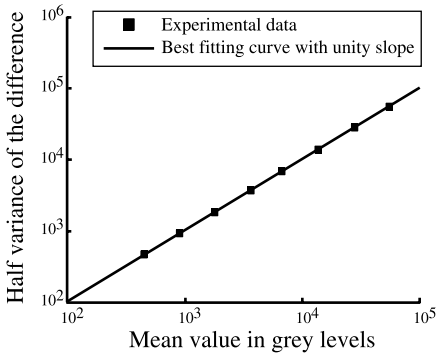

Fig. 2. Coefficient conversion from grey levels to photoelectrons. Half the variance of the difference *versus* the mean value in grey levels.

at a given intensity level and calculated the difference of the images and the variance of this difference on a wide area on the chip (about half the array). The procedure was repeated for different intensity levels over all the dynamic of the camera. In Figure 2, half the variance of the difference in grey levels is plotted on a logarithmic scale *versus* the mean intensity. The results are well fitted by a straight line with a unity slope, leading to the conclusion that the noise on this difference is Poissonian for photoelectrons. The best fit is obtained with a coefficient (inverse of the camera gain) of 0.964 photoelectron/gray level, corresponding also to the intersection of the line with the abscissa axis. This coefficient for the B-CCD camera is systematically used in the following, as well as a measured coefficient of 1.186 photoelectrons/grey level for the DDB-CCD. We have checked that this procedure gives exactly the same results for pixels after or before calibration (as defined in the next paragraph), because the difference between two identical images is directly an image of the Poissonian noise, where all the spatial noise that is reproducible from one image to the next has been eliminated by the subtraction. This reproducible spatial noise includes non uniformity of enlightening as well as non uniformity of the pixel response.

4 Spatial noise measurements and calibration of the cameras

4.1 Spatial noise measurements

We acquired shots at various beam intensities which cover the whole dynamic range of the CCD cameras. From the obtained single-shot images, we calculated the mean value and the standard deviation of the photoelectrons on a selected small area (either 5×5 pixels or 10×10 pixels wide) centered on the beam maximum. The selected area is the same for each measurement run.

The obtained plots of the standard deviation *vs.* the mean value of the photoelectrons spatial distribution are shown in Figures 3a, 4a and 5 for DDB-CCD; in Figures 3b

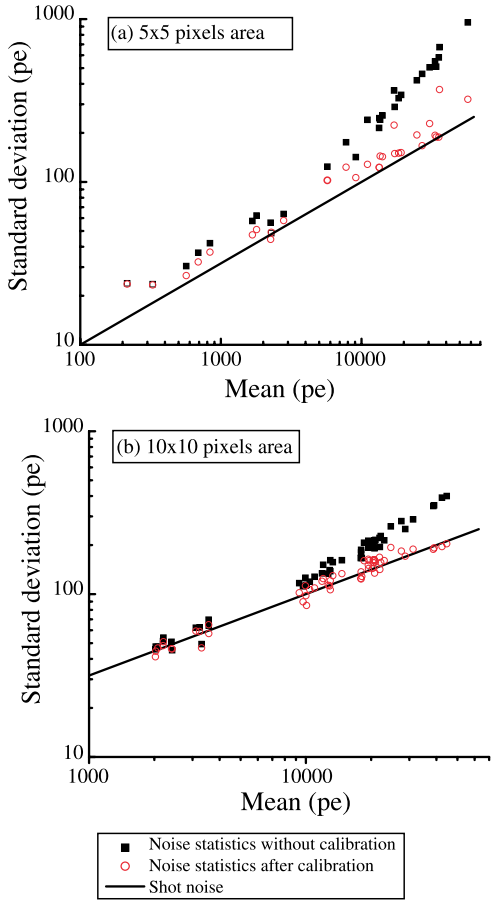

Fig. 3. Noise measurements with pulsed lasers. Standard deviation *vs.* the mean value of the photoelectrons spatial distribution for (a) DDB-CCD at 700 nm and (b) B-CCD at 527.5 nm.

and 4b for B-CCD. The depicted full line represents the expected fluctuation as predicted by the Poissonian distribution. Although the two cameras and the testing conditions are different, common features are observed in all cases. It is apparent that the Poisson statistic is satisfied only for $\overline{n} \leq 3\,000$ pe, while for large number of counting the standard deviation is larger than the expected level. To be noticed, the growth of the standard-deviation in the high-counts limit is almost linear. This suggests the presence of a classical noise source in the measurement/detection system. We devised three possible sources of noise, namely the beam profile noise, the pixel-to-pixel inhomogeneity (in gain and/or quantum efficiency) or the etaloning effect. All these causes could eventually prevent the CCD cameras to get high spatially resolved measurement, especially for high levels of photon counting. Nevertheless, in the next paragraph we show how the pixel-to-pixel inhomogeneity fully accounts for the observed deviation from theory, and a simple method to retrieve the Poissonian distribution over the whole dynamical range of the camera is presented.

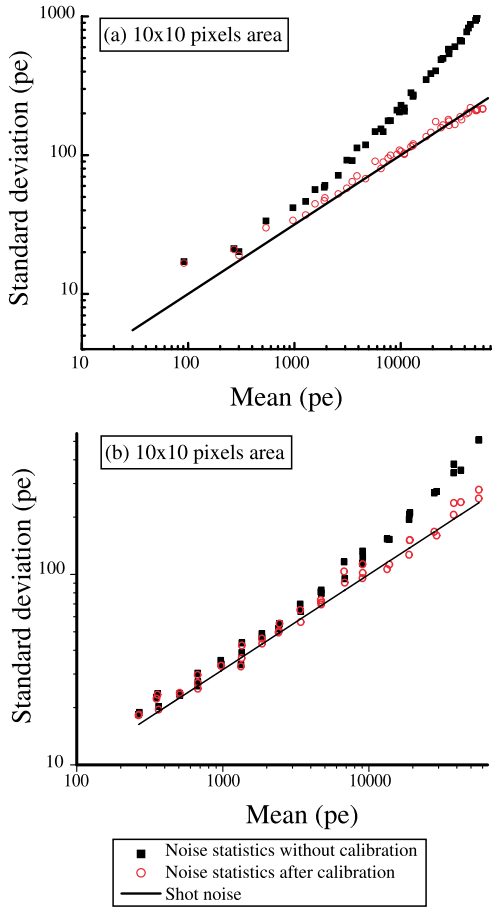

Fig. 4. Noise measurements with thermal sources. Standard deviation *vs.* the mean value of the photoelectrons spatial distribution for (a) DDB-CCD with white light source and (b) B-CCD with Hg lamp filtered with a narrow band interferential filter centered at 527.5 nm ($\Delta\lambda = 0.4$ nm).

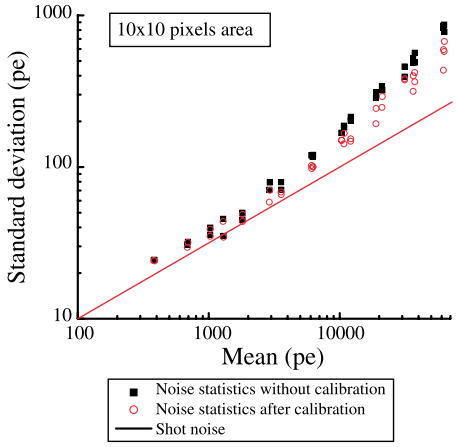

Fig. 5. Noise measurements with a continuous He–Ne laser. Standard deviation *vs.* the mean value of the photoelectrons spatial distribution for DDB-CCD.

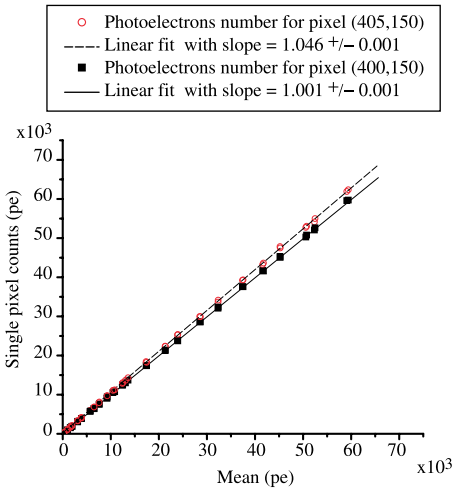

Fig. 6. Number of photoelectrons on a single pixel *versus* the mean value of photoelectron counts on the selected area for two different pixels of the DDB-CCD illuminated with pulsed laser at 700 nm.

4.2 Calibration of the cameras

To check the impact of the pixel-to-pixel inhomogeneity over the area selected for the noise measurements, we measured the calibration curves of each single pixel. Since no independent high-resolution energymeter was available, we based our measurements on a self-consistent method. Actually, for each pixel the photon counts are plotted as a function of the mean value of photoelectrons detected on the selected area (see Fig. 6). The function turns out to be linear and can be written as:

$$n_i = a_i \overline{n} + b_i, \tag{2}$$

where $\overline{n}$ is the mean number of photoelectrons on the selected area, n_i is the number of photoelectrons for the pixel i, and a_i and b_i are constants.

As shown in Figure 6, different pixels have different slopes a_i, their values being distributed around the value of 1.000 with a standard deviation of 1.8% (0.8% for the B-CCD camera). This deviation accounts for a linear increase of the spatial fluctuations of the same order of magnitude of what observed in our experiments. To subtract the effect of the pixel's inhomogeneity from the measurements, we used the measured a_i values to normalize the response of each pixel to the average response function.

We acquired a new set of images. The value of each pixel was divided by its own a_i value before the calculation of the mean counts value and the standard deviation was performed again. After this operation, we were able to recover the Poissonian statistic over the entire dynamical range of the CCD, as Figures 3 and 4 clearly show. This proves that the pixel-to-pixel inhomogeneity plays an overwhelming role among all the possible noise sources listed above.

A careful comparison between graphs in Figure 3 shows that, contrary to the case in Figure 3b, after the pixel recalibration the observed standard deviation in the case of Figure 3a is systematically higher than the expected value. We attribute this observation to the fact that the beam we used was too small compared to the selected

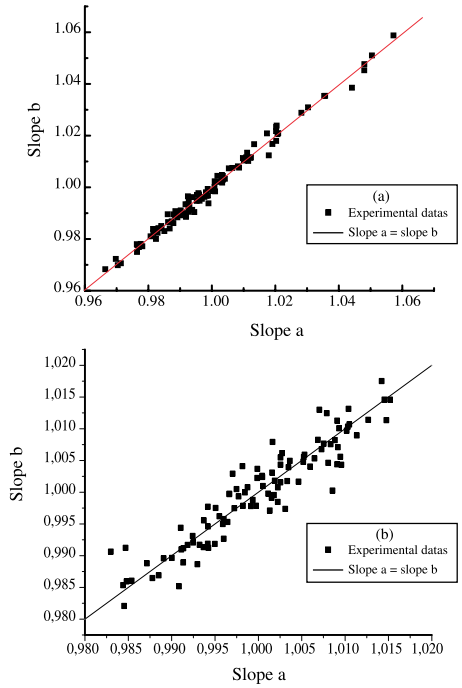

Fig. 7. For selected areas, pixels slopes calculated from one set of images *versus* the same pixels slopes calculated from an another set of images for DDB-CCD (a) and B-CCD (b).

area. In fact, a deviation from the flat field approximation as high as 9.0% is expected over such area.

For very low counting levels ($\overline{n} < 100$ pe) the measured standard deviation is also larger than expected for both CCD cameras. The recalibration has no impact on the noise level in that region. This excess noise could be accounted for by the read-out noise of the CCD which at low-light-level conditions could exceed the photon noise.

As a further proof of the importance of the pixel-to-pixel inhomogeneity contribution to the noise excess in raw data, we performed two more measurement runs with a thermal light source. The slopes a_i of each pixel's response were calculated for each run. A strong correlation between the two measurements was found, as shown in Figure 7, where the slopes of the second run are plotted *versus* of the slopes calculated with the data of the first run.

4.3 Etaloning effect

A completely different phenomenology is observed when a continuous wave light source is used instead a He–Ne laser. As apparent from Figure 5, the standard deviation measurements can not be reduced down to the shot-noise level by the application of the pixel re-calibration method. Nevertheless, the Poissonian statistics is still observed at low counting rates. A possible reason for this fact is that light with a long coherence time can induce a consistent etaloning effect [11]. Because of reflections between the parallel front and back surfaces of the CCD, fringes of equal thickness are formed in the silicon layer that acts as a partial Fabry-Perot etalon at wavelengths where silicon is semitransparent.

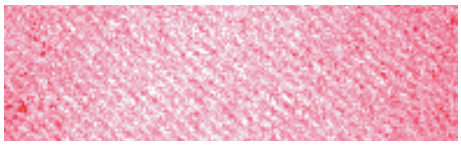

Fig. 8. Intensity map given by the DDB-CCD with a continuous He–Ne laser.

In fact, the intensity map registered by the DDB-CCD and shown in Figure 8 clearly shows a complicate pattern of interference fringes. Since the actual interference pattern strongly depends on the illumination conditions (direction of propagation, shape and phase profile of the light beam), a recovery of the actual photon statistics is not easy.

5 Statistics of the difference between shifted images of a laser beam

While Section 4 shows that the noise on a small area is Poissonian, the calibration of a wider part of the chip is necessary to compare images located at different places. For example, such a comparison is necessary to demonstrate image entanglement, *i.e.* sub-Poissonian statistics on the difference between an image and its "clone". We show in the following that the difference between two images of the same coherent laser beam recorded at two different places of the chip exhibits a nearly Poissonian statistic after calibration, while the statistic is dominated in the absence of calibration by the noise due to the pixel-to-pixel inhomogeneity. We first calibrated a wide area (400×400 pixels) around the center of the chip of the B-CCD camera by the method described in Section 4, by using the Hg lamp. The interferential filter centered on the laser wavelength prevented the response of the chip to exhibit discrepancies between the lamp and the laser. We then recorded two images of the same laser beam delivered by the Nd:YAG (Fig. 9).

The second image, selected in order to have approximately the same intensity as the first, was recorded after a lateral shift of the beam of about 15 pixels on the chip. We used the algorithm described in [13] to remove by image processing the shift in the second image. Hence, we obtained two successive images of the same laser beam, located with a subpixel precision at the same place after image processing, though different physical areas of the chip were used to record both images. We then selected a circular area with a radius of 12 pixels at the center of the beam, where the intensity profile can be considered as flat, and we computed half the variance $\sigma^2/2$ of the difference of the pixels (Fig. 9b). In the absence of classical noise, $\sigma^2/2$ should be equal to the mean of one image. The results are given in Table 1.

These results are typical and are well reproduced with other couples of images. We conclude that the residual variance due to the inhomogeneity of the pixels and to

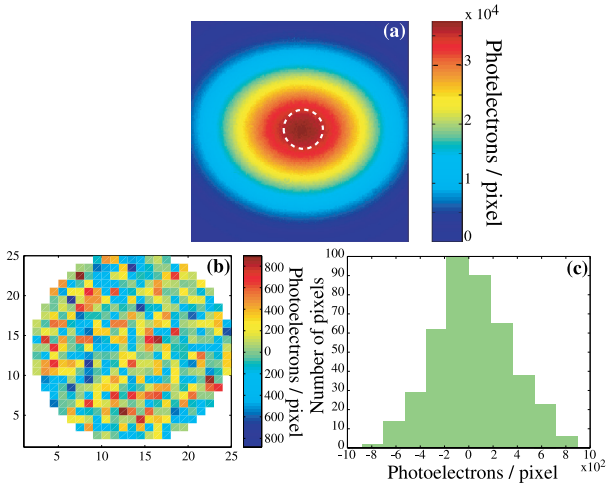

Fig. 9. (a) 200 × 200 pixels image of the Nd:YAG laser beam with the B-CCD. (b) Result of the difference between the two shifted image in the circular area represented by the dotted circle in (a). (c) Histogram of the grey levels corresponding to the (b).

Table 1. Mean value of photoelectrons in the circular area (Fig. 9a) and half of the variance on the difference between the two shifted images with and without calibration of the B-CCD camera.

	without calibration	with calibration
Mean of the intensity	36 789	36 782
$\sigma^2/2$	95 914	47 589

other unknown sources of classical noise is more than 5 times smaller after calibration. Moreover, the level of this noise decreases from twice the level of Poissonian noise to a third, opening hopes to characterize phenomena like entanglement. Before concluding this paragraph, some remarks are useful.

- First, it appears extremely difficult to obtain perfect uniform enlightening for calibration. Calibration coefficients obtained in slightly different conditions (the pinhole was replaced by a slit) exhibit differences, with a typical standard deviation of 0.3% (instead a standard deviation of the pixel response without calibration of about 0.8%). Such an uncertainty on the calibration coefficients fully explains the residual departure from a perfect Poissonian noise. Other causes could be invoked (for example, variations of the laser beam profile from one shot to another or imperfections of the shifting algorithm) but seem less plausible.
- Second, the mean intensity at the edges of the used circular area is about 5% smaller than the intensity at the top of the beam. This fact has a negligible influence on $\sigma^2/2$ because the variance is calculated on the differences between the images, unlike in Section 4 where the variance is calculated on one image.

6 Conclusion

We performed a test of the capabilities of high quantum efficiency CCD cameras to perform spatially resolved measurements of photon shot-noise. Consistent positive deviations from the expected spatial Poisson distribution were observed for high average counting levels of the photoelectrons. Experiments show that the gain inhomogeneity of pixels on the CCD chip fully accounts for this excess noise, provided that the etaloning effects are negligible (short coherence time of the light source). We have demonstrated that the expected Poissonian statistics could be recovered if a calibration of the single-pixel gain is performed on the CCD area. If the Poissonian character of the noise from an image to another (equivalent to the time domain noise) was experimentally verified some years ago (see for example [14]), spatial fluctuations in one image were scarcely studied until this paper. Though all light sources in this paper are completely classical, we believe that retrieving the shot-noise in the full dynamic range of the cameras paves the way to spatially resolved photon noise measurements at the sub shot noise level, a necessary step to demonstrate quantum properties of images.

This work has been supported in part by the European Union (QUANTIM contract IST-2000-26019). Y. Jiang would like to thank the Young Scientist Innovation Funds from Fujian Province (2001j008) for partial support.

References

1. S.K. Choi, M. Vasilyev, P. Kumar, Phys. Rev. Lett. **83**, 1938 (1999)
2. M.I. Kolobov, L.A. Lugiato, Phys. Rev. A **52**, 4930 (1995)
3. I.V. Sokolov, M.I. Kolobov, L.A. Lugiato, Phys. Rev. A **60**, 2420 (1999)
4. A. Gatti, E. Brambilla, L.A. Lugiato, M.I. Kolobov, Phys. Rev. Lett. **83**, 1763 (1999)
5. T.B. Pittman D.V. Strekalov, D.N. Klyshko, M.H. Rubin, A.V. Sergienko, Y.H. Shih, Phys. Rev. A **53**, 2804 (1996)
6. M.I. Kolobov, Rev. Mod. Phys. **71**, 1539 (1999)
7. M.I. Kolobov, I.V. Sokolov, Sov. Phys. JETP **69**, 1097 (1989)
8. I. Marzoli, A. Gatti, L.A. Lugiato, Phys. Rev. Lett. **78**, 2092 (1997)
9. A. Gatti, E. Brambilla, L.A. Lugiato, M. Kolobov, J. Opt. Soc. Am. B **1**, 1 (1999)
10. R. Loudon, *The quantum theory of light*, 2nd edn. (Oxford Science Publications, Oxford, 1983)
11. J.R. Janesick, *Scientific Charge-Coupled Devices* (SPIE Press Bellingham, Washington, 2001), pp. 204-205, see also Roper Scientific website `http://www.roperscientific.de/theory.html`
12. L. Mandel, E. Wolf, *Optical Coherence and Quantum Optics* (Cambridge University, New York 1995), pp. 727-733
13. C. Poilane, E. Lantz, G. Tribillon, P. Delobelle, Eur. Phys. J. Applied Physics **11**, 131 (2000)
14. J.R. Janesick, T. Elliott, S. Collins, M.M. Blouke, J. Freeman, Opt. Eng. **26**, 692 (1987)